arXiv:1612.00572v1 [cond-mat.mes-hall] 2 Dec 2016

Mechanisms for strong anisotropy of in-plane g-factors in hole based quantum point contacts

D. S. Miserev[1], A. Srinivasan[1], I. Farrer[2], D. A. Ritchie[3], A. R. Hamilton[1], O. P. Sushkov[1]
[1] *School of Physics, University of New South Wales, Sydney, Australia*
[2] *Department of Electronic and Electrical Engineering, University of Sheffield, United Kingdom and*
[3] *Cavendish Laboratory, University of Cambridge, United Kingdom*
(Dated: December 5, 2016)

In-plane hole g-factors measured in quantum point contacts based on p-type heterostructures, strongly depend on the orientation of the magnetic field with respect to the electric current. This effect, first reported a decade ago and confirmed in a number of publications, has remained an open problem. In this work, we present systematic experimental studies to disentangle different mechanisms contributing to the effect and develop the theory which describes it successfully. We show that the most important mechanism for the anisotropy is related to the existence of two kinematically different Zeeman effective interactions for holes.

PACS numbers: 71.70.Ej, 73.22.Dj, 71.18.+y

A quantum point contact (QPC) is a narrow quasi-1D constriction linking two 2D electron or hole system reservoirs. It is essentially the simplest mesoscopic system which makes it interesting both for technological applications and on a fundamental level. Experimental studies of QPCs started with the discovery of the conductance quantization in steps of $G_0 = 2e^2/h$ [1, 2]. The steps are due to the quantization of transverse channels [3]. Effects of many-body interactions/correlations in QPCs

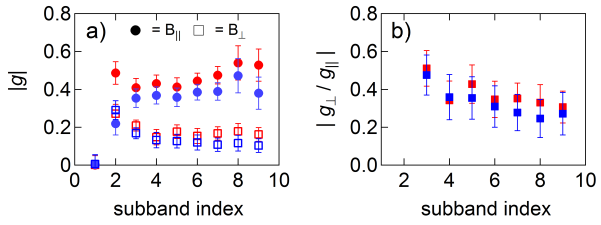

FIG. 1: g-factors measured experimentally in the present work. The hole number density in the 2D reservoirs is $n = 1.1 \cdot 10^{11}$ cm^{-2}. a): Absolute values of subband g-factors. The circles (squares) correspond to the direction of magnetic field along (perpendicular) the QPC. b): The ratio $|g_\perp/g_{||}|$ versus the subband index. In the both panels red (blue) symbols correspond to the out-of-plane electric field in quantum well $E_\infty = 1.2 \cdot 10^6$V/m ($E_\infty = 2.5 \cdot 10^6$V/m).

were subsequently identified in "0.7-anomaly" of the conductance and g-factor enhancement [4], and a few years later, in zero bias anomaly of the conductance [5]. Since the first measurement [4], g-factors in n-type QPCs have been measured in numerous experiments, relatively recent one is reported in Ref. [6]. The electron g-factor is enhanced compared to its bulk value due to the exchange Coulomb interaction between electrons and due to the non-equilibrium way of measurement in QPCs [7].

The in-plane electron g-factor in a QPC is isotropic, i.e. it takes the same value for any direction of the in-plane magnetic field. Even in electron systems such as InGaAs which has appreciable spin-orbit coupling no in-plane g-factor anisotropy has been observed [4, 8]. Contrary to this, measurements for holes in QPCs based on GaAs p-type heterostructures [9–11] indicate a huge anisotropy, the value of the g-factor for the direction of magnetic field along the QPC, $g_{||}$ is typically larger than that for the perpendicular direction, $g_\perp$, see Fig.1.

While, in principle, some g-factor anisotropy is possible because of the strong hole spin-orbit interaction (SOI), the mechanism behind the observed effect remains unclear. One mechanism to explain the g-factor anisotropy was suggested in Ref. [10]. The idea is based on the crystal anisotropy of the cubic lattice. This mechanism does contribute to the g-factor anisotropy. However, theoretical estimations as well as the direct optical experiment [12] show that though this contribution is important, it is still too small to describe the measured effect.

In this work, we identify a new mechanism for the g-factor anisotropy unrelated to the crystal lattice. This mechanism is negligible at very low hole densities. However, at real physical densities this is the major anisotropy mechanism. Previous measurements were performed using 2D hole systems formed at a single heterojunction [9, 10], which can be modeled as a triangular potential well. There was also a measurement with an asymmetric quantum well [11] which can be modeled as a square potential with an electric field along the z-axis. The z-axis is perpendicular to the plane of the 2D hole system. Strong z-asymmetry results in the Rashba SOI [13] which is cubic in the momentum for hole systems [14–16]. To disentangle effects of Rashba SOI from other spin-orbital effects, in the present work we perform measurements of QPC g-factors for GaAs heterostructures of the quantum well design. The hole gas is confined in a 15nm rectangular quantum well. An external electric field E_z is superimposed on the well using an in-situ back gate below the quantum well. Due to the split-gate the configuration of E_z near the QPC is quite complex, see

discussion in the supplementary material. To avoid ambiguity we characterize the electric field by its value far away from the QPC, E_∞. We show data for the values of back gate bias that correspond to $E_\infty = 1.2 \cdot 10^6$V/m (more symmetric) and $E_\infty = 2.5 \cdot 10^6$V/m (less symmetric). The actual electric field E_z at the neck of the QPC is proportional to E_∞, but somewhat smaller. The measured absolute values of g-factors are presented in Fig.1a. Other experimental details are provided in the supplementary material.

There was also a measurement, Ref. [11], performed for a 15nm quantum well with the hole density $n = 3 \cdot 10^{11}$ cm^{-2}. According to our estimates this density corresponds to the electric field $E_\infty \sim 3.1 \cdot 10^6$V/m. In this case $g_\perp$ is almost zero for all subbands. We explain this result here, as well.

Fig.1 demonstrates that a significant g-factor anisotropy is present even in a quantum well with relatively low electric field. Also the anisotropy reaches its maximal value at some particular electric field when the transverse in-plane g-factor vanishes [11]. Another observation is that in all the cases both g-factors are very small for the lowest transverse channel, n=1.

In our theoretical analysis the direct Coulomb interaction of holes is included in the QPC self-consistent field. It is commonly believed that the exchange interaction of holes in 2D heterostructures is relatively weak due to the multicomponent structure of hole wave functions. More importantly, this interaction can hardly contribute to the g-factor anisotropy because it does not have a spin-orbit nature. So, in our analysis we disregard the exchange hole-hole interaction. Non-interacting holes in bulk conventional semiconductors are described by the Luttinger Hamiltonian [17]. We consider here only the spherical approximation [18]

$$H_L = \left(\gamma_1 + \frac{5}{2}\overline{\gamma}_2\right)\frac{\mathbf{p}^2}{2m} - \frac{\overline{\gamma}_2}{m}\left(\mathbf{p}\cdot\mathbf{S}\right)^2 \ , \qquad (1)$$

where $\mathbf{p}$ is 3D quasi-momentum; $\mathbf{S}$ is the spin $S = 3/2$; γ_1, $\overline{\gamma}_2 = (2\gamma_2 + 3\gamma_3)/5$ are Luttinger parameters; m is the free electron mass. There is also a non-spherical part of the Luttinger Hamiltonian that depends on the cubic lattice orientation. It is proportional to $\gamma_2 - \gamma_3$. In materials with large SOI $\gamma_2 \approx \gamma_3$ and, therefore, we neglect this term here. It is worth noting that a mechanism of the g-factor asymmetry suggested in Ref. [10] is based on the non-spherical part of the Hamiltonian.

A quantum well potential $W(z)$ imposed on (1) confines dynamics along the z-axis leading to 2D sub-bands. Here, we consider only the lowest sub-band with dispersion

$$H_0 = \varepsilon_{\boldsymbol{k}} \ , \qquad (2)$$

where $\boldsymbol{k} = (k_x, k_y) = (p_x, p_y)$ is the 2D momentum. Projection of spin on the z-axis S_z is a good quantum number. Due to the negative sign of the second term in (1), the lowest band is a Kramers doublet with $S_z = \pm 3/2$. The standard way to describe the Kramers doublet is to introduce the effective spin $s = 1/2$ with related Pauli matrices $\boldsymbol{\sigma}$. The correspondence at $k = 0$ is very simple: $|\uparrow\rangle = |S_z = 3/2\rangle$, $|\downarrow\rangle = |S_z = -3/2\rangle$. Note that the effective spin operators $\sigma_\pm = \sigma_x \pm i\sigma_y$ are flipping $S_z = \pm 3/2$ projections. Hence, $\sigma_\pm$ are transformed as $S^3_\pm$.

Consider a symmetric quantum well, $W(z) = W(-z)$, with imposed in-plane magnetic field $\mathbf{B}$. The kinematic structure of the effective two-dimensional Zeeman (linear in B) Hamiltonian has the following form [19]

$$\begin{aligned} H_Z = &- \frac{1}{4}\overline{g}_1(k)[B_+k_+^2\sigma_- + B_-k_-^2\sigma_+] \\ &- \frac{1}{4}\overline{g}_2(k)[B_-k_+^4\sigma_- + B_+k_-^4\sigma_+] \\ g_1 = &\ k^2\overline{g}_1(k) \ , \quad g_2 = k^4\overline{g}_2(k) \ . \end{aligned} \qquad (3)$$

Pauli matrices $\sigma_\pm$ has the angular momentum selection rule $\Delta J_z = \pm 3$, and $B_\pm$ corresponds to $\Delta J_z = \pm 1$. The powers of $k_\pm$ in (3) balance the z-component of the angular momentum in such a way that the total Hamiltonian conserves the angular momentum, $\Delta J_z = 0$. While the g_1-term in (3) is well known, the g_2-term has never been considered before. In standard perturbative treatment of the Luttinger Hamiltonian (1) the g_2-term appears only in a rather high order of the perturbation theory. Of course at small momenta $g_2 \ll g_1$, however, at physicaly relevant momenta they are comparable. We will show that the existence of two different kinematic structures in the Zeeman interaction (3) is the major reason for the QPC g-factor anisotropy.

The effective momentum dependent g-functions $g_1(k)$ and $g_2(k)$ have been calculated recently [19] for symmetric heterostructures. These functions for an infinite rectangular GaAs quantum well of width d=15nm are plotted in Fig.2a by black lines.

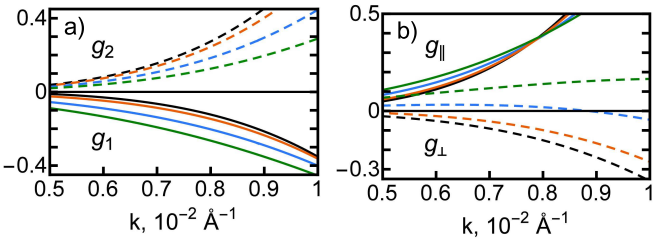

FIG. 2: a): Functions g_1 (solid lines) and g_2 (dashed lines) versus momentum, see Eq.(3). b): Functions $g_{||}$ (solid lines) and $g_\perp$ (dashed lines) versus momentum, see Eq.(4). Both panels correspond to a rectangular infinitely deep GaAs quantum well of width d=15nm with a superimposed electric field E_z. We present plots for four values of E_z: $E_z = 0$ (black), $E_z = 0.5 \cdot 10^6$ V/m (red), $E_z = 1 \cdot 10^6$ V/m (blue), and $E_z = 1.5 \cdot 10^6$ V/m (green).

The magnetic g-factor is determined experimentally by the splitting of the transconductance peaks in a magnetic

field. We direct the x-axis along the QPC (the direction of the current) and the y-axis perpendicular to the QPC. The transconductance peaks correspond to the chemical potential aligning with the top of the QPC barrier, where $k_x = 0$. Therefore, in the g-factor measurements $k = k_y$ and $k_+ = ik$, $k_- = -ik$. Hence, at the 1D subband edge the Zeeman interaction (3) for a QPC reads

$$\begin{aligned} H_Z \;\rightarrow\; & -\frac{1}{2} g_{||} B_x \sigma_x - \frac{1}{2} g_{\perp} B_y \sigma_y \qquad (4) \\ & g_{||}(k) = g_2 - g_1 \\ & g_{\perp}(k) = -g_2 - g_1 \ . \end{aligned}$$

The in-plane g-factors $g_{\|}$ and $g_{\perp}$ are different and this is the mechanism of the g-factor asymmetry. Plots of $g_{||}(k)$ and $g_{\perp}(k)$ for a 15nm rectangular GaAs quantum well are presented in Fig.2b by black lines.

Our experiments have been performed with 2D hole density of $1.1 \cdot 10^{11}\text{cm}^{-2}$. This corresponds to the Fermi momentum $k_F = 0.83 \cdot 10^{-2}\text{Å}^{-1}$. Transverse QPC channels are determined by the "transverse" Hamiltonian

$$H_{tr} = \varepsilon_k + U(y) \ , \quad k = k_y \ , \qquad (5)$$

where $U(y)$ is the transverse self-consistent potential of the QPC created by the split-gate. Energy levels of the Hamiltonian (5), E_n, enumerated by index $n = 1, 2, 3, ...$, correspond to the transverse channels. Variation of the gate voltage adjusts the self-consistent potential $U(y)$ providing the condition to depopulate n^{th} 1D subband.

$$E_n = \varepsilon_F \ . \qquad (6)$$

This implies that $U(y)$ depends on n. The self-consistent potential has been calculated previously, see e.g. Ref. [20]. The potential is parabolic for small n, and becomes rectangular for larger n. To fit the numerically calculated potential, we use the following parametrization

$$U(y) = U_0 \left(1 - \frac{\exp[-a^2/d^2] + 1}{\exp[(y^2 - a^2)/d^2] + 1} \right), \qquad (7)$$

where $U_0 = 10$ meV, d=17nm, and the value of a is adjusted to satisfy the condition (6). The potential for $n = 1, 4, 7$ is plotted in Fig.3a. While the precise shape of the potential is not very important, the condition

$$U(0) \approx 0 \qquad (8)$$

is essential. Of course this condition is not exact and can depend on a particular design of the QPC. The condition is very natural for large subband indexes while for small indexes one should expect $U(0) > 0$. Assuming (8) and the rectangular shape of $U(y)$, see Fig.3a, we conclude that the transverse momentum at the QPC is equal to the Fermi momentum in 2 reservoirs, $k = k_F = 0.83 \cdot 10^{-2}\text{Å}^{-1}$. Hence, from Fig.2b (black lines) we find that g-factors are independent of the subband index and the values are $g_{||} = 0.45$, $g_{\perp} = -0.15$. These values are in good agreement with the data in Fig.1a, note that the experiment does not determine signs of g-factors. Obviously, vanishing of experimental g-factors for $n = 1$ is related to a violation of (8). Here $U(0) > 0$, hence $k < k_F$, and g-factors drop dramatically at small k.

Using techniques developed in Ref. [19] we also perform numerical calculations for the wire potential (7). The corresponding Hamiltonian reads

$$\begin{aligned} H \;&=\; H_L + W(z) + U(y) - 2\kappa \, \boldsymbol{B} \cdot \boldsymbol{S} \\ \boldsymbol{A} \;&=\; [B_y(z - z_0), -B_x(z - z_0), 0] \ , \qquad (9) \end{aligned}$$

where $\boldsymbol{A}$ is the vector potential included in H_L via "long derivatives", for details see Ref. [19], 2κ is the bulk g-factor, z_0 is an arbitrary constant. Due to gauge invariance, z_0 cannot affect any physical results as it corresponds to a constant in-plane vector potential, $\boldsymbol{A}_0 = -z_0[\boldsymbol{B} \times \hat{\boldsymbol{z}}]$, that can be gauged out by shift of the momentum, $\boldsymbol{k} \rightarrow \boldsymbol{k} - \boldsymbol{A}_0$. We set $z_0 = 0$ to have the minimum of the dispersion (2) at $\mathbf{k} = 0$. This choice is valid for any symmetric heterostructure $W(z) = W(-z)$.

The longitudinal momentum is zero, $k_x = 0$. This is due to the n^{th} 1D subband depopulation and due to the gauge choice $z_0 = 0$. Hence, the wave function of the Hamiltonian (9) depends only on z and y. Brute force numerical diagonalization of Eq. (9) yields the g-factors directly. We keep the conditions (6) and (8) in our calculations. The corresponding g-factors for $k_F = 0.83 \cdot 10^{-2}\text{Å}^{-1}$ ($\epsilon_F \approx 2$meV) are plotted in Fig.3b

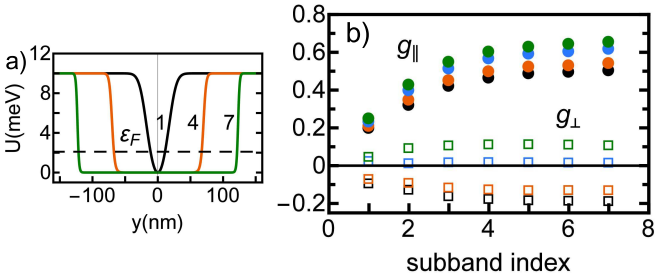

FIG. 3: a): QPC transverse potential for three different channels $n = 1, 4, 7$. b): QPC g-factors calculated within the quantum wire model for different transverse channels n. The heterostructure is the infinite rectangular quantum well of 15nm width with superimposed electric field E. The hole density in leads is $1.1 \cdot 10^{11}$ cm^{-2}. Circles (squares) represent $g_{\|}$ ($g_{\perp}$). Four different values of E_z are considered: $E_z = 0$ (black), $E_z = 0.5 \cdot 10^6$ V/m (red), $E_z = 1 \cdot 10^6$ V/m (blue), $E_z = 1.5 \cdot 10^6$ V/m (green).

by black symbols (circles and squares). Even with the condition (8), g-factors are smaller at low n since the potential $U(y)$ becomes parabolic, and the expectation value of k_y^2 is smaller for the parabolic potential than for the rectangular one. Overall, for the symmetric quantum well in GaAs we have excellent agreement between theory and experiment.

Now we turn to the asymmetric heterostructure, $W(z) \neq W(-z)$. The following kinematic structure in the effective Hamiltonian becomes possible: $(\mathbf{S}\cdot\mathbf{k})^2(\hat{\mathbf{z}}\cdot[\mathbf{k}\times\mathbf{S}])$, where $\hat{\mathbf{z}}$ is the unit vector along the z-axis. After projection to the $S_z = \pm 3/2$ sub-space, it yields the Rashba SOI

$$H_R = -\frac{i}{2}\alpha_k(k_+^3\sigma_- - k_-^3\sigma_+) \ . \tag{10}$$

This term has to be added to the effective 2D Hamiltonian (2),(3). Besides the Rashba SOI (10) an asymmetric quantum well gives rise to the following term in the effective 2D Hamiltonian

$$H_B(\mathbf{k}) = \gamma_k([\mathbf{B}\times\mathbf{k}]\cdot\hat{\mathbf{z}}) \ . \tag{11}$$

Here, γ_k is a momentum dependent coefficient. This spin independent term can be absorbed in the dispersion, $\varepsilon_{\mathbf{k}} + H_B(\mathbf{k}) \approx \varepsilon_{\mathbf{k}+\mathbf{q}}$, where $\mathbf{q} = -m^*(k)\gamma_k[\mathbf{B}\times\hat{\mathbf{z}}]$ and $m^*(k) = k/\left(\frac{\partial\varepsilon_k}{\partial k}\right)$ is the effective mass.

The gauge condition for asymmetric heterostructures is similar to the symmetric ones: we set the dispersion minimum at $\mathbf{k} = 0$. On the level of effective Hamiltonian it is equivalent to $\gamma_{k=0} = 0$, see Eq.(11). The value of z_0 providing this condition follows from the equation

$$\left\langle \left(\frac{\partial H_L}{\partial \boldsymbol{k}}\right)_{\boldsymbol{k}=0} \right\rangle = \left.\frac{\partial H_{2D}}{\partial \boldsymbol{k}}\right|_{\boldsymbol{k}=0} = 0 \ . \tag{12}$$

Here H_L is the Luttinger Hamiltonian (1) accounting for the "long" electromagnetic derivatives, $\mathbf{p} \to \mathbf{p} - \mathbf{A}$. We use the gauge condition (12) in all our calculations. This condition guaranties that the 1D subband depopulation occurs at $k_x = 0$. Certainly, $z_0 \neq 0$ for asymmetric heterostructures.

It is worth noting that in the case of an asymmetric quantum well the gauge invariance of the 2D effective Hamiltonian is less trivial than in the case of a symmetric quantum well. For example, the constant shift $\boldsymbol{k} \to \boldsymbol{k} - \boldsymbol{A}_0$, $\boldsymbol{A}_0 = -z_0[\boldsymbol{B}\times\hat{\mathbf{z}}]$, leads to the regauging of all magnetic couplings: $\gamma_k \to \gamma_k - z_0/m^*$, $\bar{g}_1 \to \bar{g}_1 + z_0(6\alpha_k + k\alpha_k')$, $\bar{g}_2 \to \bar{g}_2 - z_0\alpha_k'/k$. Here α_k' is the derivative of the Rashba coupling coefficient. It is worth noting that there is no regauging of $\bar{g}_1$, $\bar{g}_2$ for symmetric quantum wells where the Rashba coefficient is zero, $\alpha_k = 0$. On the other hand, when the Rashba SOI is non-zero one can get non-zero values of $\bar{g}_1$, $\bar{g}_2$ even at $\mathbf{B} = 0$ by introducing a constant vector-potential $\mathbf{A}_0$. Apparently, this is a nonphysical effect related to the shift of the dispersion minimum. To avoid these complications, it is very important to choose the gauge (12) that results in $g_1(k)$ and $g_2(k)$ which have direct physical meaning.

The values of electric field $E_\infty = 1.2\cdot 10^6$V/m and $E_\infty = 2.5\cdot 10^6$V/m were calculated using a 1D electrostatic model. The actual electric field E_z at the neck of the QPC is proportional to E_∞, but somewhat smaller, see the supplementary material. To describe the situation within a relatively simple theoretical model, we just introduce a uniform electric field $E_z \sim 10^6$V/m superimposed on the infinite rectangular well. Note that 10^6V/m is a very strong electric field resulting in the variation of the potential within the quantum well width larger than the heavy-light hole energy splitting. The calculated g-functions for $E_z = 0.5$, $E_z = 1$, and $E_z = 1.5$ (units of 10^6V/m) are plotted in Fig.2b. From this figure, we see that the longitudinal g-factor $g_\parallel$ is not very sensitive to the electric field, meanwhile the transverse one, $g_\perp$, changes dramatically. It increases with electric field starting from negative values at $E_z = 0$ and crossing zero at $E_z \approx 1\cdot 10^6$V/m. In experiment Ref. [11] $g_\perp$ is zero. We have performed an electrostatic calculation and found that in conditions of Ref. [11] $E_\infty \approx 3.1\cdot 10^6$V/m. From here we conclude that $E_z \sim (0.3 \div 0.5)E_\infty$. The decreasing of the ratio $|g_\perp/g_{||}|$ with electric field is consistent with our data presented in Fig.1b.

Besides the $g_1 - g_2$-effect considered above, there is one more effect influencing $g_\perp$ in the z-asymmetric heterostructures. The effect appears as a direct consequence of the Rashba interaction. It leads to $g_\perp$ oscillations/suppression with subband number, $\propto \frac{\sin \pi n\delta}{\pi n\delta}$, where δ is a parameter related to Rashba SOI. At the same time, $g_\parallel$ is not affected. This effect is weak in quantum wells and hence, it is almost irrelevant to our experiments. Still it is an interesting effect and we discuss it in the supplementary material. A similar effect was previously addressed in numerical calculations for hole wires [21]. Also, a somewhat similar effect exists in electron systems [22].

Similarly to the symmetric well, we also perform a brute force numerical diagonalization of the quantum wire problem with Hamiltonian (9) and the gauge condition (12). This calculation accounts both the $g_1 - g_2$-effect and the Rashba effect discussed in the previous paragraph. The calculated g-factors for $k_F = 0.83\cdot 10^{-2}$Å^{-1} are plotted in Fig.3b. Unlike the experiment, see Fig.1a, the theoretical value of $g_{||}$ slightly grows with electric field. This is probably because the condition (8) is slightly violated in our QPCs. Most significant the asymmetry between $g_\perp$ and $g_{||}$ is enhanced by electric field, and this is perfectly consistent with the experimental data.

In conclusion We have performed systematic experimental and theoretical studies to resolve the problem of anisotropic g-factors measured in quantum point contacts based on p-type heterostructures. We found that the most important mechanism for the anisotropy is related to the existence of two kinematically different effective Zeeman interactions for holes. There is also a small additional contribution to the anisotropy related to the Rashba interaction in strongly asymmetric heterostructures.

We thank Tommy Li and Stefano Chesi for important

discussions. The device used in this work was fabricated using facilities of the NSW Node of the Australian National Fabrication Facility. The work has been supported by the Australian Research Council grant DP160103630.

[1] B. J. van Wees, H. van Houten, C. W. J. Beenakker, J. G. Williamson, L. P. Kouwenhoven, D. van der Marel, and C. T. Foxon, Phys. Rev. Lett. **60**, 848 (1988).
[2] D. A. Wharam, T. J. Thornton, R. Newbury, M. Pepper, H. Ahmed, J. E. F. Frost, D. G. Hasko, D. C. Peacock, D. A. Ritchie, and G. A. C. Jones, J. Phys. C: Solid State Phys. **21**, L209 (1988).
[3] M. Büttiker, Phys. Rev. B **41**, 7906 (1990).
[4] K. J. Thomas, J. T. Nicholls, M. Y. Simmons, M. Pepper, D. R. Mace, and D. A. Ritchie, Phys. Rev. Lett. **77**, 135 (1996).
[5] S. M. Cronenwett, H. J. Lynch, D. Goldhaber-Gordon, L. P. Kouwenhoven, C. M. Marcus, K. Hirose, N. S. Wingreen, and V. Umansky, Phys. Rev. Lett. **88**, 226805 (2002).
[6] A. M. Burke, O. Klochan, I. Farrer, D. A. Ritchie, A. R. Hamilton, and A. P. Micolich, Nano Lett. **12**, 4495 (2012).
[7] G. Vionnet and O. P. Sushkov, Phys. Rev. Lett. **116**, 126801 (2016) .
[8] T. P. Martin, A. Szorkovszky, A. P. Micolich, A. R. Hamilton, C. A. Marlow, R. P. Taylor, H. Linke, and H. Q. Xu, *Phys. Rev. B* **81**, 041303(R) (2010).
[9] J. C. H. Chen, O. Klochan, A. P. Micolich, A. R. Hamilton, T. P. Martin, L. H. Ho, U. Zülicke, D. Reuter and A. D. Wieck, *New J. Phys.* **12**, 033043 (2010).
[10] Y. Komijani, M. Csontos, I. Shorubalko, U. Zülicke, T. Ihn, K. Ensslin, D. Reuter and A. D. Wieck, *EPL* **102**, 3 (2013).
[11] F. Nichele, S. Chesi, S. Hennel, A. Wittmann, C. Gerl, W. Wegscheider, D. Loss, T. Ihn, and K. Ensslin, *Phys. Rev. Lett.* **113**, 046801 (2014).
[12] X. Marie, T. Amand, P. Le Jeune, M. Paillard, P. Renucci, L. E. Golub, V. D. Dymnikov, and E. L. Ivchenko Phys. Rev B **60**, 5811 (1999).
[13] Yu. A. Bychkov and E. I. Rashba, Sov. Phys. JETP Lett. **39** (1984).
[14] S. Chesi, G. F. Giuliani, L. P. Rokhinson, L. N. Pfeiffer, and K. W. West, *Phys. Rev. Lett.* **106**, 236601 (2011).
[15] R. Winkler, D. Culcer, S. J. Papadakis, B. Habib, and M. Shayegan, *Semicond. Sci. Technol.* **23**, 114017 (2008).
[16] F. Nichele, A. N. Pal, R. Winkler, C. Gerl, W. Wegscheider, T. Ihn, and K. Ensslin, *Phys. Rev. B* **89**, 081306(R) (2014).
[17] J. M. Luttinger, *Phys. Rev* **102**, 1030 (1956).
[18] A. Baldereschi and N. O. Lipari, *Phys. Rev. B* **8**, 2697 (1973).
[19] D. S. Miserev and O. P. Sushkov, arXive:1610.03169.
[20] A. Siddiki and F. Marquardt, Phys. Rev. B **75**, 045325 (2007).
[21] M. M. Gelabert and L. Serra, Phys. Rev. B **84**, 075343 (2011).
[22] K. Kolasinski, A. Mrenca-Kolasinska, and B. Szafran, *Phys. Rev. B* **93**, 035304 (2016).